An Evaluation of Particle Filters for Contact-SLAM Problems

Shuai Li[1], Siwei Lyu[2], Jeff Trinkle[1], and Wolfram Burgard[3]

[1]Department of Computer Science, Rensselaer Polytechnic Institute
[2]Department of Computer Science, University at Albany, SUNY
[3]Department of Computer Science, University of Freiburg

***Abstract*—The contact-SLAM problem is a broad class of grasping and manipulation problem and it is very important to robotic manipulation tasks, particularly when contacts are likely to be intermittent. Several researchers have developed particle filters for C-SLAM problems that estimate the state of manipulated objects, some geometric properties, and their contacts, but the effects of various designing issues are obfuscated by implementation details and are not discussed thoroughly. In this paper, we study the C-SLAM problem restricted to the contact normal direction to understand fundamental modeling choices through analysis of real and simulated experiments. We compare the results of both rigid body and compliant body model with several sources of noise to give users guidance in implementing particle filters for C-SLAM problems.**

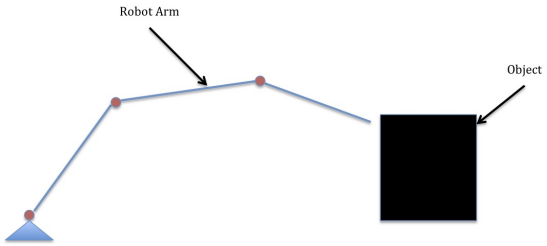

Fig. 1: Robot arm moving into contact with an object.

I. Introduction

The SLAM problem is central to robot autonomy. Applying the SLAM mind-set to contact problems defines the Contact-SLAM (C-SLAM) problem, which tracks manipulated object, locations of contacts as they form and break, and possibly also estimates geometric parameters of the object. In the C-SLAM problem, estimating geometric parameters is analogous to constructing a map in the SLAM problem, since localizing the object relative to the hand and estimating contact locations is strongly influenced by object geometry.

The motion of solid bodies in contact is well described by Newton-Euler differential equations and complementarity conditions [1]. This model is highly nonlinear which makes linear filtering techniques, such as Kalman filter, not applicable. Due to the success of particle filters in nonlinear SLAM problems and their simplicity and flexibility, they are good candidates to solve the C-SLAM problem [2]. In this paper, we focus on some design aspects of particle filters for the C-SLAM.

A. Previous Work using Particle Filter in C-SLAM

Gadeyne et. al. [3] considered the object localization problem of a rectangular box using a force-controlled arm with a look-up table, which eliminates low probability samples from the particle filter. Hebert et. al. [4] used a stereo camera and force/torque sensor to estimate the pose of a rectangular box held by a Barrett Hand. Unlike our work, these works did not incorporate object dynamics into the state transition model. Zhang et. al. [5] did include object dynamics, but only considered a rigid body model and one and noise model in their filter. In this work, we compare rigid and compliant contact models and several noise sources to gain insight into their impact on filter performance.

Recently, there has been a number of applications exploring improvement of particle filters for C-SLAM problems. Zhang et. al. [6] developed a general solution by fitting a dynamic Bayesian network into a Rao-Blackwellized particle filter to speed up C-SLAM. Duff et. al. [7] incorporated a real-time physics simulator into a particle filter to estimate the poses of objects with dynamics and intermittent contact. Koval et. al. [8] derived a "manifold particle filter," which improves particle generation for the quasistatic push-grasping. These works make suggestions on modifying the dynamic model and trying different noise models, however, the two perspectives were not combined as they are in our paper.

The contribution of this paper is the comparison of different models of object dynamics with contact and different noise models on particle performance in C-SLAM problems. Results from physical experiments and simulation are presented.

II. Deterministic Contact Dynamics Models

In this paper, we will focus on object tracking and identifying the binary contact state; contact or no contact. As shown in Fig. 1, consider a robot arm moving into contact with an object. The dynamics of the arm and object expressed in the workspace can be written as follows: [9]:

$$\tilde{M}(\theta)\ddot{x} = \tilde{J}^T\lambda + \tilde{D}(\theta,\dot{\theta}) \quad (1)$$

$$0 \le \lambda \perp \Psi(x) \ge 0, \quad (2)$$

where θ is the vector of manipulator joint angles, λ is the contact force and moment, $\tilde{M}(\theta)$ is the combined arm/object

inertia matrix, $\tilde{J}$ is the jacobian associated with the contact constraints, and $\tilde{D}(\theta, \dot{\theta})$ is the vector of all other forces including joint friction, Coriolis, and centripetal forces mapped into the workspace. The second line of equation (1) is known as a complementarity condition. The condition and the $\perp$ symbol will be explained below.

A. Rigid Body Model

Since we are primarily interested in the contact transition, in the remainder of this paper, we use a simplified version of the model by considering the dynamics only in the direction of the robot's approach toward the object (the x-direction). Further, we assume that joint friction and the arm velocity are small enough so that the effects of $\tilde{D}$ may be neglected. Under these restrictions, we consider two widely used contact models: a rigid body model and a compliant contact model.

Applying the approach in [10] to our problem yields the following dynamic model for the rigid body case, which takes the form a linear complementarity problem:

$$mv_{t+1} = u_t h - \lambda_{t+1} h + mv_t \quad (3)$$

$$x_{t+1} = v_{t+1} h + x_t \quad (4)$$

$$\Psi_{t+1} = x_{\text{wall}} - x_{t+1} \quad (5)$$

$$0 \leq \lambda_{t+1} \perp \Psi_{t+1} \geq 0. \quad (6)$$

where Ψ is the signed distance between the robot and the wall and the $\perp$ symbol connotes orthogonality. The last condition is known as the normal complementarity condition, which is really three conditions: $\lambda_{t+1} \geq 0$, $\Psi_{t+1} \geq 0$, and $\Psi_{t+1}\, \lambda_{t+1} = 0$; contact forces are compressive, no penetration is allowed, and the contact force is nonzero if and only if the robot touches the wall.

B. Compliant Body Model

Defining λ_{t+1} as a function of Ψ_t converts the rigid body model into one with contact compliance. In this paper, we use a nonsmooth version of the Voigt-Kelvin contact model defined in [11]. Letting $\delta = -\Psi$ be the depth of penetration and K and C be the contact stiffness and damping, then the contact model is:

$$\delta_t = max\{0, -\Psi_t\} \quad (7)$$

$$\dot{\delta}_t = \frac{1}{h}\left[max\{0, -\Psi_t\} - max\{0, -\Psi_{t-1}\}\right] \quad (8)$$

$$\lambda_{t+1} = max\{0, K\delta_t + C\dot{\delta}_t\} \quad (9)$$

Equations (7-9) replace complementarity condition equation (6), so the dynamic model with compliance consists of equations (3,4,7,8,9).

III. Probabilistic Models

Probabilistic models are needed in order to implement a particle filter. We define our probabilistic models as follows:

$$z_{t+1} = F(z_t, u_t + \epsilon_t) + \eta_{t+1}, \quad (10)$$

where F is the state transition model and $z_t = [x_t\ v_t]^T$ is the state variable. ϵ_t and η_{t+1} are while Gaussian noise affecting the actuator input and the future state estimation respectively. We only observe the position of the block, which makes our observation model,

$$o_{t+1} = G(z_{t+1}) + \gamma_{t+1}, \quad (11)$$

where $G(z_{t+1}) = x_{t+1}$ and γ_{t+1} is a white Gaussian noise.

IV. Filters

In this paper, we use a *SIR* particle filter [2], which is summarized in Algorithm 1 with the state transition model in Algorithm 2, to estimate the state of the robot arm. We then combine *SIR* particle filter with the two probabilistic models from section III, which yields a *noisy input particle filter (NIPF)* anda *noisy state particle filter (NSPF)*. *NSPF* can compensate some of the modeling errors by using the noise term. However using it, can generate predictions that violate the physical constraints of the dynamic models. To deal with this side effect, we define *projected particle filter (PJPF)* which give additional weights to particles according to their projected distances to the complementarity plane. In addition, we introduce *force state particle filter (FSPF)* to deal with noisy F/T sensors. *FSPF* treats the applied force as a state variable and F/T sensor readings as its observations. The state transition model of the applied force used is:

$$u_{t+1} = u_t + w_t \quad (12)$$

where w_t is a white Gaussian noise.
In the subsequent experiments, we use 150 particles, which we found achieves a good balance between computation time and accuracy.

Algorithm 1 SIR Particle Filter

function FILTER(Z_t, u_t, o_{t+1}, w_t)
  $\bar{Z}_{t+1}$, $\bar{w}_{t+1}$ = UPDATE_STATE(Z_t, u_t, N,w_t)
  if resample condition satisfied **then**
    for $i = 1 \rightarrow N$ **do**
      Draw j with probability $\propto \bar{w}_{t+1}^{[j]}$
      $Z_{t+1}^{[i]}$ = $\bar{Z}_{t+1}^{[j]}$, $w_{t+1}^{[i]}$ = $\frac{1}{N}$
    end for
  else
    $Z_{t+1} = \bar{Z}_{t+1}$, $w_{t+1} = \bar{w}_{t+1}$
  end if
  return Z_{t+1}, w_{t+1}
end function

Algorithm 2 SIR Particle Filter Update State

function UPDATE_STATE(Z_t, u_t, N, w_t)
  for $i = 1 \rightarrow N$ **do**
    $\bar{Z}_{t+1}^{[i]}$ =DETER_STATE_TRANSIT($Z_t^{[i]}, u_t$)
    $\bar{w}_{t+1}^{[i]} = P(o_{t+1}|\bar{Z}_{t+1}^{[i]}) \cdot w_t^{[i]}$
  end for
  Normalize $\bar{w}_{t+1}$
  return $\bar{Z}_{t+1}$, $\bar{w}_{t+1}$
end function

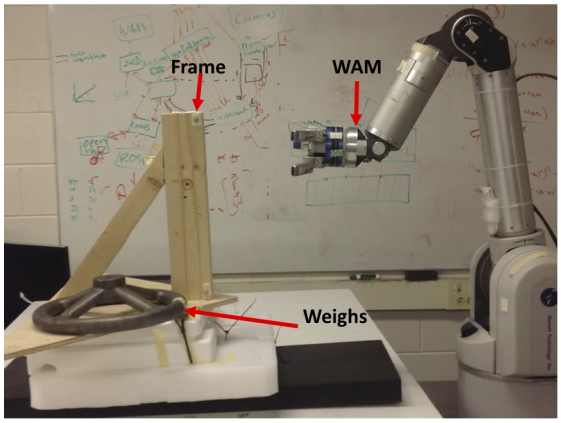

Fig. 2: Physical experiment.

V. Experiments

We perform both virtual and physical experiments. The physical experiments were done with a Barrett WAM whose palm move into contact with a stiff wall with guarded control(see Fig. 2). In the virtual experiments, the WAM is modeled as a rigid block moved by an external force toward a rigid wall.

We divided the estimation task into two stages: robot tracking and contact prediction. During the tracking stage (prior to contact), the dynamic models are linear, so the particle filters were compared to each other and to Kalman filters. For the contact prediction stage, Kalman filters could not be used, so the particle filters were are compared only against each other. Contact confidence (the sum of the weights of the particles that are in contact) was used as the performance criterion.

A. Tracking Results

The dynamics for the tracking stage is linear and the contact dynamic models do not have effect at this stage. As can be seen from Fig. 3, all filtering methods performs very similarly on tracking tasks in the virtual experiments. However in the physical experiments (Fig. 4), *SIR* diverge from the actual trajectory soon after tracking starts while other filtering methods perform similarly. This is because the F/T sensor readings from Barrett WAM have a non-zero mean Gaussian noise. This noise diverge the estimation. As soon as the states of all the particles are ”far away“ from the actual trajectory, the degeneracy of the particle filter happens and all particles except one particle die, which is also the reason that *SIR* particle filter has a much smoother estimation after its divergence. Another observation is that different ways of adding noise do not have effect on the tracking stage. However, the noise level needs to be picked carefully to have good tracking results. Typically, lower noise level will favor the state transition model and higher noise level will favor the observation model.

B. Contact Prediction Results

Contact confidence is used to evaluate the performance of the contact prediction. From Fig. 5 and Fig. 6, we can see that in the virtual experiments all the filtering methods show a boost of the contact confidence very close to the actual contact. Then *SIR* particle filter with rigid body model as well as *SIR* particle filter, *NIPF* and *FSPF* with compliant body model show consistence of the contact confidence. When the contact is about to happen, all particles have a big magnitude velocity due to the acceleration of the external force. Therefore, when the contact happens, most of the particles will contact the wall, which explains the boost of the contact confidence. After the contact, the particles are either stopped or slowed down by the contact forces. Then the noise will vibrate the particles around the contact boundary. The results of this effect are different between rigid body model and compliant body model. In rigid body model, the vibration causes penetration and the particles are shoot away from the boundary by the impulse generated by the penetration, which explains the major drop of contact confidence for *NSPF* and *PJPF*. In the compliant body model, however, the particles are moved back to the boundary ”gently“ by the compliant constraint. Also we observe that *NIPF* and *FSPF* performs significantly better than *NSPF* and *PJPF* in the rigid body model case. The reason for this is that *NIPF* and *FSPF* do not break the physical constraints and therefore all the particles that penetrate the wall will be pushed back to the contact boundary, which increases the contact confidence.

For the physical experiments in Fig. 7 and Fig. 8, only *FSPF* and *NIPF* give acceptable contact prediction (*SIR* particle filter predict contact far ahead of actual contact as a result of the divergence). Again, the reason explained in the virtual experiment results has a big effect in the physical experiment results. This shows that when the input force signal is very noisy, *FSPF* and *NIPF* are the best choices among all the filtering methods. The rigid body model and compliant body model do not perform very differently and the compliant body model performs slightly better. However, even though *SIR* particle filter makes bad contact prediction, its behavior shows that the compliant body model makes the contact prediction smoother than the rigid body model. The reason is that there is a non-zero mean Gaussian noise in the input force signal which will cause the particles to vibrate around the contact boundary. But the non-zero mean of the noise actually pushes the particles to penetrate the wall and creates a buffer for the particles, which reduces the the vibration in the contact prediction.

References

[1] J.C. Trinkle, J.S. Pang, S. Sudarsky, and G. Lo. On Dynamic Multi-Rigid-Body Contact Problems with Coulomb Friction. *ZAMM - Zeitschrift für Angewandte Mathematik und Mechanik*, 77(4):267–279, 1997.

[2] W. Burgard S. Thrun and D. Fox. *Probablistic Robotics*.

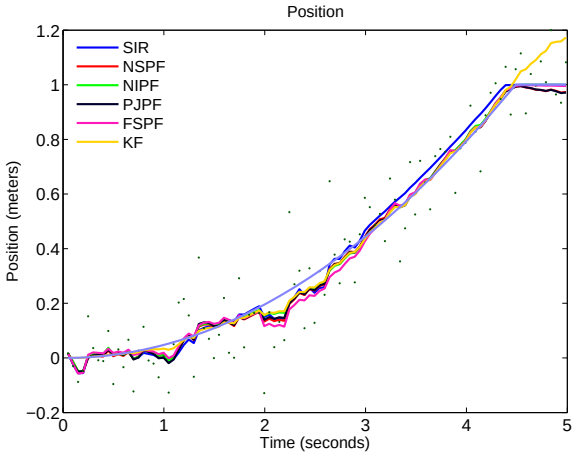

Fig. 3: Tracking results of the virtual experiments.

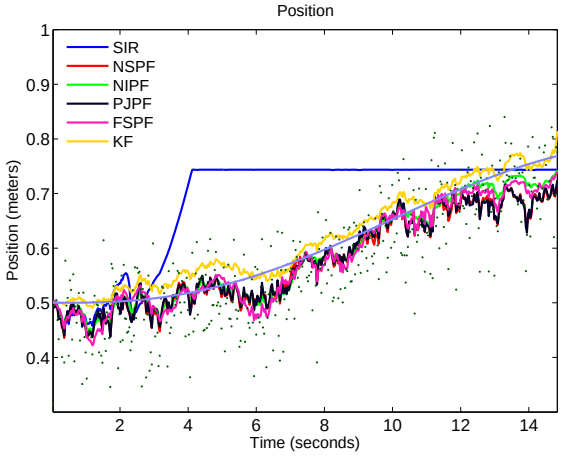

Fig. 4: Tracking results of the physical experiments.

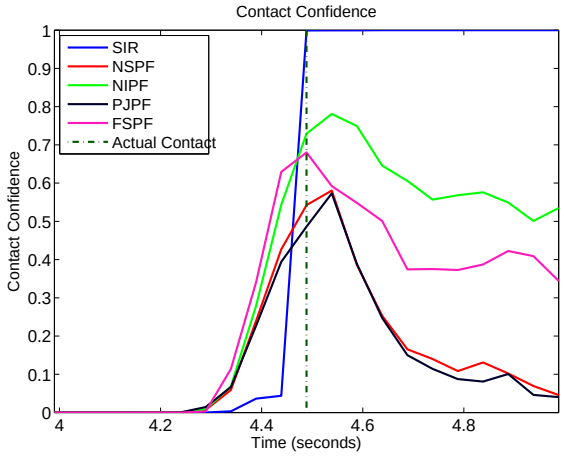

Fig. 5: Contact prediction of the virtual experiments, rigid body model.

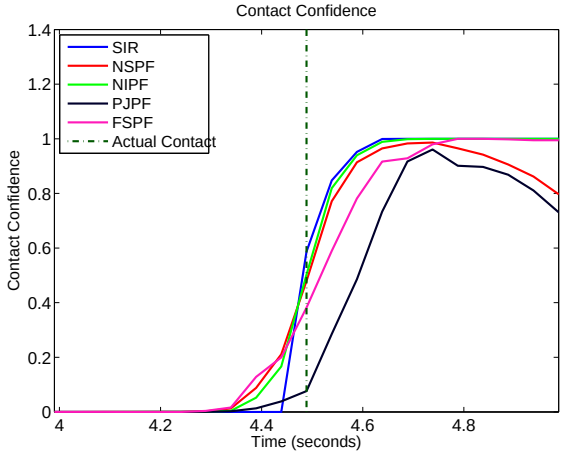

Fig. 6: Contact prediction of the virtual experiments, compliant body model.

The MIT Press, Cambridge, Massachusetts, London, England, 2006.

[3] K. Gadeyne and H. Bruyninchx. Markov techniqus for object localization with force-controlled robots. In *IEEE International Conference on Robotics and Automation(ICRA)*, 2001.

[4] P. Hebert et al. Fusion of stereo vision, force-torque, and joint sensors for estimation of in-hand object location. In *IEEE International Conference on Robotics and Automation*, 2011.

[5] L. Zhang and J.C. Trinkle. The Application of Particle Filtering to Grasp Acquistion with Visual Occlusion and Tactile Sensing. In *IEEE International Conference on Robotics and Automation*, May 2012.

[6] L.E. Zhang, S. Lyu, and J.C. Trinkle. A Dynamic Bayesian Approach to Real-Time Estimation and Filtering in Grasp Acquisition. In *IEEE International Conference on Robotics and Automation (ICRA)*, May 2013.

[7] D. Duff et al. Physical simulation for monocular 3D model based tracking. In *IEEE International Conference on Robotics and Automation*, 2011.

[8] N. S. Pollard M. C. Koval, M. R. Dogar and S. S. Srinivasa. Pose Estimation for Contact Manipulation with Manifold Particle Filters. In *IEEE International Conference on Robotics and Automation (ICRA)*, 2013.

[9] R. M. Murray, Z. Li, and S. S. Sastry. *A Mathematical Introduction to Robotic Manipulation*. CRC Press, 1994.

[10] D.E. Stewart and J.C. Trinkle. An Implicit Time-Stepping Scheme for Rigid Body Dynamics with Inelastic Collisions and Coulomb Friction. *International Journal of Numerical Methods in Engineering*, 39, 1996.

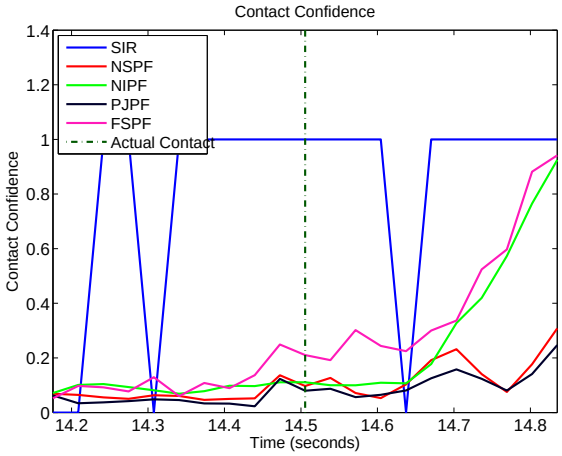

Fig. 7: Contact prediction of the physical experiments, rigid body model.

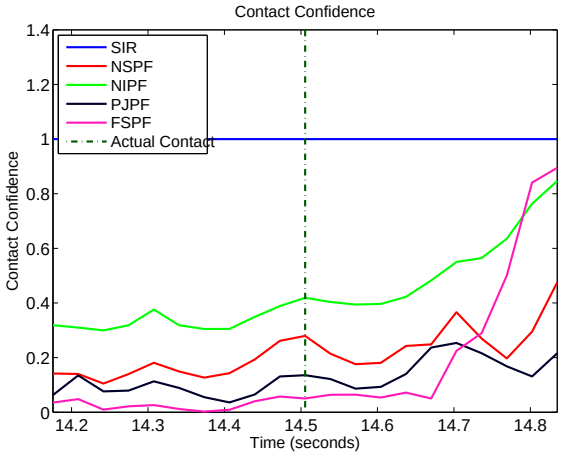

Fig. 8: Contact prediction of the physical experiments, compliant body model.

[11] Peng Song. Modeling, analysis and simulation of multi-body systems with contact and friction, 2002.